Icarus 205 (2010) 605–618

Contents lists available at ScienceDirect

Icarus

journal homepage: www.elsevier.com/locate/icarus

Detecting active comets in the SDSS

Michael Solontoi [a,*], Željko Ivezić [a], Andrew A. West [b], Mark Claire [a], Mario Jurić [c], Andrew Becker [a], Lynne Jones [a], Patrick B. Hall [d], Steve Kent [e], Robert H. Lupton [c], Gillian R. Knapp [c], Tom Quinn [a], James E. Gunn [c], Don Schneider [f], Craig Loomis [c]

[a] University of Washington, Department of Astronomy, Box 351580, Seattle, WA 98195, USA
[b] MIT Kavli Institute for Astrophysics and Space Research, 77 Massachusetts Ave., Cambridge, MA 02139-4307, USA
[c] Princeton University Observatory, Princeton, NJ 08544, USA
[d] Department of Physics and Astronomy, York University, 4700 Keele St., Toronto, ON, Canada M3J 1P3
[e] Fermi National Accelerator Laboratory, Batavia, IL 60510, USA
[f] Department of Astronomy and Astrophysics, Pennsylvania State University, University Park, PA 16802, USA

ARTICLE INFO

Article history:
Received 13 February 2009
Revised 17 July 2009
Accepted 24 July 2009
Available online 12 August 2009

Keywords:
Comets
Photometry
Comets, Coma

ABSTRACT

Using a sample of serendipitously discovered active comets in the Sloan Digital Sky Survey (SDSS), we develop well-controlled selection criteria for greatly increasing the efficiency of comet identification in the SDSS catalogs. After follow-up visual inspection of images to reject remaining false positives, the total sample of SDSS comets presented here contains 19 objects, roughly one comet per 10 million other SDSS objects. The good understanding of selection effects allows a study of the population statistics, and we estimate the apparent magnitude distribution to $r \sim 18$, the ecliptic latitude distribution, and the comet distribution in SDSS color space. The most surprising results are the extremely narrow range of colors for comets in our sample (e.g. root-mean-square scatter of only $\sim$0.06 mag for the $g - r$ color), and the similarity of comet colors to those of jovian Trojans. We discuss the relevance of our results for upcoming deep multi-epoch optical surveys such as the Dark Energy Survey, Pan-STARRS, and the Large Synoptic Survey Telescope (LSST), and estimate that LSST may produce a sample of about 10,000 comets over its 10-year lifetime.

1. Introduction

The small bodies of the Solar System offer a unique insight into its early stages and evolution. Only a few locations still exist where samples of the original solid materials of the solar nebula remain: the main Asteroid belt, the Trojan populations of the giant planets, the Kuiper Belt just outside the orbit of Neptune, and, far beyond the planets, the objects in the Oort Cloud. Today these populations can be studied as asteroids and comets. Understanding these populations, both physically and in their number and size distributions, is a key element in testing various theories of Solar System formation and the evolution of our planetary system. Comets sample the two farthest regions of the Solar System, the Kuiper Belt and the Oort Cloud; regions whose great distances make in situ studies difficult, and in the case of the Oort Cloud, beyond our current observational capabilities.

Comets are defined as objects that have activity: the ejection by out-gassing of small amounts of dust and gas, typically at small heliocentric distances. These materials interact with the solar wind and radiation, leading to the production of cometary coma and tails. Most comets belong to one of two main dynamical groups: the Jupiter family comets (JFC), generally with low-inclination, prograde orbits, thought to originate in the reservoir of the Kuiper Belt, and long period comets (LPC), whose orbits include a wide range of inclinations and directions, with aphelia far beyond the planets of the Solar System. A common method used to separate the JFC, LPC and asteroidal orbits is the use of the Tisserand parameter with respect to Jupiter (Levison and Duncan, 1997). This requires a comet to have a well characterized orbit, so it cannot be used for comets with only single epoch observations, nor can it distinguish the comets residing within the main Asteroid belt (Hsieh and Jewitt, 2006) from the population of main-belt asteroids.

Most photometric studies of comets to date have targeted select groups of known comets, often in only one or two filters, to look for activity levels at various heliocentric distances, and to make estimates of their physical properties (Lowry et al., 1999, and references therein). Other studies of known comets have focused on spectroscopy, or the use of narrow-band filters, to estimate physical properties and investigate the gas species (A'Hearn et al., 1995, and references therein). While these targeted surveys make great contributions to cometary science, they do not offer the opportunity to study an unbiased, selection of comets, apart from limits imposed by flux and angular size resolution; or to answer questions about the number of comets on

* Corresponding author. Fax: +1 206 685 0403.
E-mail address: solontoi@astro.washington.edu (M. Solontoi).

0019-1035/$ - see front matter © 2009 Elsevier Inc. All rights reserved.
doi:10.1016/j.icarus.2009.07.042

the sky at a given time, and their distributions in magnitude, heliocentric distance and angular size.

As opposed to these targeted observations, all-sky surveys for small Solar System bodies such as the Lincoln Near-Earth Asteroid Research (LINEAR) detect vast numbers of Solar System objects including comets (Stokes et al., 2000). These detections and cometary discoveries build up excellent catalogs of object populations for study, but these surveys have not had the ability to observe the comets in multiple filters.

The Sloan Digital Sky Survey (SDSS; York et al., 2000) offers an opportunity to observe a large number of comets in multiple filters. By the fifth public data release (DR5) almost 8000 deg^2 of sky has been imaged (Adelman-McCarthy et al., 2007), thus allowing detection of both known and here to fore unknown comets for population studies, as well as providing accurately calibrated five-color photometry. These data can be used for determining the physical properties of the comets imaged by the survey. The SDSS also allows direct comparison with other populations of small bodies (NEOs, Main-Belt Asteroids, Trojans) imaged by the survey, all having been observed by the same instrument and calibrated to the same standards.

While searching for known comets in the SDSS data could produce a list of comets for detailed study, the ability to "mine" SDSS for comets is a way to turn it into a discovery survey as well. A method must be developed that can select comets using the measured SDSS catalog parameters. Such a method could allow both known and undiscovered comets to be found in SDSS, and also inform methods for detecting new comets in the upcoming next generation of large area surveys (e.g. Pan-STARRS and LSST, Kaiser et al., 2002; Ivezić et al., 2008).

Active comets are not easily identified in the SDSS imaging catalogs. Given the sky coverage and the numbers of known comets on the sky, it is expected that a few dozen comets may have been imaged by the survey. Selecting a complete sample from the 215 million object DR5 catalog without significant contamination is not trivial. A basic selection criteria requires that active comets are resolved objects, and that they have a statistically significant angular velocity measurement. However, selection criteria designed to be sensitive to comets out to Jupiter's orbit select about 1% of the SDSS galaxies, about 1 million objects. While most comets can be efficiently recognized in SDSS images via visual inspection, a sample of $\sim$1 million candidates is too large to visually examine. These "false positives" could be easily rejected if a "second epoch" of images were available, but over most of the survey area the SDSS obtained only one epoch of data. We therefore develop methods based on the use of SDSS Galaxy spectroscopy as "second epoch" data as well as restricted search criteria in velocity and color space which can be used to prune the candidate list down to a number that is manageable for visual inspection.

In Section 2, we present and test selection criteria for identifying objects from the Sloan Digital Sky Survey catalogs that may be active comets. The analysis of the resulting sample of 19 confirmed comets, including the sample magnitude, sky and color distributions, is described in Section 3, and we discuss our results in Section 4. In the remainder of this paper, which focuses on selection methods, we use cataloged parameters automatically computed by the SDSS processing pipelines. In a sequel to this paper, we will present an analysis of SDSS data based on custom photometry of the individual observations.

2. Methodology

2.1. An overview of SDSS

The SDSS is a digital photometric and spectroscopic survey which covered about one quarter of the Celestial Sphere in the North Galactic cap and a smaller $\sim$(300 deg^2) but much deeper survey in the Southern Galactic hemisphere and began standard operations in April 2000 (Stoughton et al., 2002; Abazajian et al., 2003; Abazajian et al., 2004; Abazajian et al., 2005; Adelman-McCarthy et al., 2006). SDSS is using a dedicated 2.5 m telescope (Gunn et al., 2006) to provide homogeneous and deep (r < 22.5) photometry in five band-passes (Fukugita et al., 1996; Gunn et al., 1998; Smith et al., 2002; Hogg et al., 2001; Tucker et al., 2006) repeatable to 0.02 mag (root-mean-square scatter, hereafter rms, for sources not limited by photon statistics, Ivezić et al., 2003) and with a zero-point uncertainty of $\sim$0.02–0.03 mag (Ivezić et al., 2004). The flux densities of detected objects are measured almost simultaneously in five bands (*u, g, r, i*, and *z*) with effective wavelengths of 3540 Å, 4760 Å, 6280 Å, 7690 Å, and 9250 Å. The large survey sky coverage has resulted in photometric measurements for well over 100 million stars and a similar number of galaxies.[1] The completeness of SDSS catalogs for point sources is $\sim$99.3% at the bright end and drops to 95% at magnitudes of 22.1, 22.4, 22.1, 21.2, and 20.3 in *u, g, r, i*, and *z*, respectively. Astrometric positions are accurate to better than 0.1 arc-second per coordinate (rms) for sources with r < 20.5 (Pier et al., 2003), and the morphological information from images allows reliable star–Galaxy separation to r $\sim$ 21.5 (Lupton et al., 2002; Scranton et al., 2002). A compendium of the technical details about SDSS can be found on the SDSS web site (http://www.sdss.org), which also provides interface for the public data access.

The samples presented in this paper are based on the SDSS Fifth Public Data Release, hereafter DR5 (Adelman-McCarthy et al., 2007), which ran through June 2005. Detailed information about this data release including sky coverage, changes from previous data releases and data quality statistics can be found at http://www.sdss.org/DR5, and in Adelman-McCarthy et al., 2007.

2.2. Moving objects in SDSS

The SDSS, while mainly designed for observations of extragalactic objects, is significantly contributing to studies of the Solar System, notably in the success it has had with asteroid detections, cataloged in the SDSS Moving Object Catalog (hereafter SDSS MOC, Ivezić et al., 2001). This public, value added catalog of SDSS asteroid observations contains, as of its fourth release, measurements of 471,000 moving objects, 220,000 of which were matched to 104,000 known asteroids from the ASTORB file.[2] The quality of SDSS MOC data was discussed in detail in Ivezić et al. (2001), Jurić et al. (2002), and Parker et al. (2008).

The footprint of DR5 in ecliptic coordinates is shown in Fig. 1. SDSS avoids the galactic plane, which is limited in its use for Solar System work due to the crowded stellar background. The survey covers the sky at and near the ecliptic from approximately $\lambda = 100$–225°. The repeated scans of the Southern Galactic hemisphere (crossing $\lambda = 0^\circ$) also run through the ecliptic. This uneven coverage with regards to ecliptic latitude is addressed in Section 3.3.

The SDSS camera (Gunn et al., 1998) uses a drift-scanning technique along great circles and detects objects in the order *r, i, u, z, g*, with detection in two successive bands separated in time by 72 s with the different bands registered to the same coordinate system using stationary stars (Pier et al., 2003). Moving objects appear to have their color centers separated when color composite images are made, and if moving sufficiently rapidly will appear as streaks

[1] The fifth public data release (DR5) covers almost 8000 deg^2 of sky, and includes catalog of 215 million objects (Adelman-McCarthy et al., 2007); see http://www.sdss.org/dr5. The most recent seventh data release includes 357 million unique objects.

[2] See ftp://ftp.lowell.edu/pub/elgb/astorb.html.

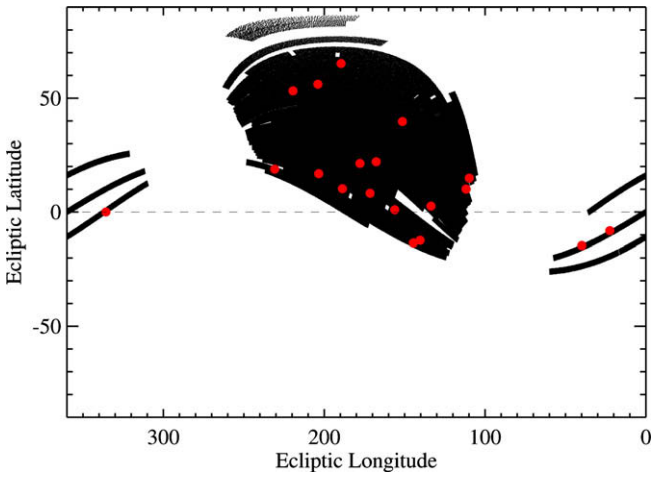

Fig. 1. The foot print of SDSS DR5 in ecliptic coordinates. The great circle scans of the survey avoid the Galactic plane and are limited to approximately Galactic latitude $b > 30°$. The disconnected stripes running through $\lambda = 0°$ is the Southern Galactic survey. The red dots show the positions of the comets found in SDSS as discussed in this paper. (For interpretation of the references to colour in this figure legend, the reader is referred to the web version of this article.)

of individual colors. An angular velocity, calculated from the astrometrically-calibrated image centroids in each filter, is calculated for every photometric object. Asteroids in SDSS typically appear as unresolved (star-like) sources (a sequence of dots or streaks, see Fig. 2). Comets are relatively easy to visually distinguish from other sources; an active comet is typically a resolved source, with color separation visible in the near nuclear coma, and is surrounded by a diffuse coma and sometimes tail(s). Fig. 2 shows examples of a comet and an asteroid imaged by SDSS.

2.3. SDSS magnitudes and processing flags

Unless otherwise specified, the magnitudes presented here are so-called model magnitudes. These are designed for Galaxy photometry, and are determined by accepting the better of a de Vaucouleurs and an exponential profile of arbitrary size and orientation (see Stoughton et al., 2002). The surface brightness profile of a comet differs from that of a Galaxy, and thus these model magnitudes may not be optimal for comet studies. We will present analysis based on custom photometry in a future paper. In this work, we limit our analysis to cataloged parameters computed by the SDSS photometric pipeline (Lupton et al., 2002). A comparison between the measured surface brightness profile of the observed Comet 30P Reinmuth and these Galaxy models is discussed is Section 3.5.

All objects detected by the SDSS photometric pipeline have several other magnitudes measured (for each of the five bands). The *PSF magnitude* is measured by fitting the point spread function model to the object. For a resolved object such as a comet or Galaxy this does not measure all of the flux. The *Petrosian magnitude* is designed to measure extended, resolved objects, and provides a model-independent measurement for resolved galaxies. Petrosian magnitudes are a good choice for nearby bright galaxies, or in our case large comets. However, because we will be dealing with comets down to the brightness where the Petrosian magnitudes become less reliable, we have made the choice of citing model magnitudes unless otherwise specified. For details on how these magnitudes are measured by SDSS and the advantages of each, please see Stoughton et al. (2002), and references therein.

In addition to assigning magnitudes, the SDSS photometric pipeline deblends complex or overlapping objects into component pieces and then reports photometry on these "children" of the original, or "parent", object. All the processing steps taken by the photometric pipeline are encoded in an extensive series of processing flags. These flags indicate the status of each object, record image defects (saturation, bad pixels, etc.), and warn of possible problems in the measurement of various quantities associated with the object.[3] The deblending process, designed to provide measurements of each object in an overlapped image, can sometimes divide a single resolved object into several. Especially for images of complex, extended objects like comets, the processing flags are vital for proper identification and measurement.

2.4. The initial sample

The first SDSS comet was found serendipitously (Comet C/1999 F2 Dalcanton; Dalcanton et al., 1999), while examining candidate irregular galaxies. Beyond Comet Dalcanton there have been several other serendipitously found comets. Five were found by visually inspecting the images as they were processed. This method can only discover the largest objects, because fainter, smaller comets are not usually immediately noticeable in large images (SDSS fields measure 9×13 arc min^2). Four additional comets were found by comparing Galaxy spectra and photometry. Since active comets are classified as galaxies by the SDSS photometric pipeline, they can be targeted for spectroscopic follow-up. By the time the follow-up spectra are taken (typically several weeks or more) the comet will no longer be at that position in the sky, resulting in a blank-sky spectrum. Visual inspection of the photometric images revealed that these resolved objects were indeed comets because they exhibited detectable motion during the 5 min of imaging.

While these serendipitous detections prove the concept of using SDSS to find and study comets, a robust completeness estimate requires a systematic approach to find comets from a single epoch imaging set, using a well-defined single data release of the survey. To do so, we first systematically searched for comets using SDSS Galaxy spectroscopy as a second-epoch information source. Due to the design of the SDSS spectroscopic Galaxy targeting algorithm (Strauss et al., 2002), this search is flux-limited to $r \leqslant 17.7$ (Petrosian magnitude). Out of the 440,502 ($r \leqslant 17.7$ Petrosian) spectroscopic galaxies in DR5, 6771 have spectra that are inconsistent with galactic spectral classification (representing about 1.5% of the targeted galaxies' spectra). Images of these 6771 objects were visually inspected and eight comets were found in this sample. We used $50 \times 50''$ color composites (jpg) available from the SDSS DR5 site[4] for visual identification. These eight comets contained two new comet detections: all four comets found previously by comparing Galaxy spectra to photometry, and two of the five comets serendipitously identified in images. Comet Dalcanton and two of the five visually identified comets could not have been found as they are not in imaging runs that were released as part of DR5. The last unrecovered comet had been targeted for spectra, but had not yet been followed up at the time of DR5's publication. Table 1 summarizes these results.

Comets brighter than the spectroscopic limit ($r \leqslant 17.7$ Petrosian) are easily visually recognizable, and if inspected should only be missed due to SDSS image overlap (see Section 3.1.) Due to the small number of bright comets it is unlikely but possible that a comet was not selected for spectra due to being too close to another object (see Strauss et al., 2002) for details on the limits of completeness for galaxies in the SDSS spectroscopic survey).

While this is a robust method for finding comets in SDSS catalogs, it does not fully utilize SDSS imaging data due to the spectro-

[3] For more details about SDSS processing flags see http://www.sdss.org/dr5/products/catalogs/flags.html.

[4] http://cas.sdss.org/astrodr5/en/tools/chart/list.asp.

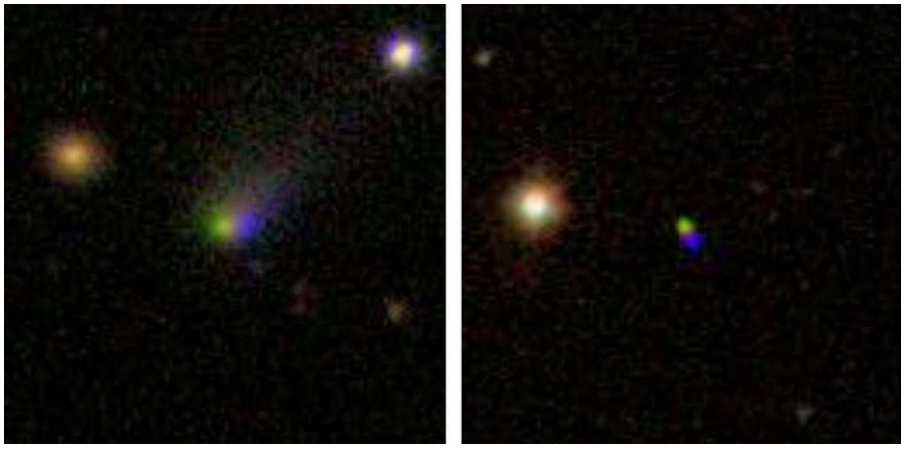

Fig. 2. A three color (*g*, *r*, and *i*) composite of Comet P/1999 V1 Catalina (left) and Asteroid 2006 SP_{363} (right) as imaged by SDSS. The images show the effect of the motion of Solar System objects during observation by the SDSS camera. Each image is a $50'' \times 50''$ square downloaded as jpg's from the SDSS sky server.

Table 1
The comets initially found in the SDSS along with their method of discovery. Of these 12 detections, four do not have spectroscopic follow-up in SDSS. Accidental Spectra refers to the four comets serendipitously discovered while examining galactic spectra (see Section 2.4). The Notes column offers the reasons for why not all of the comet positions in question were not found in SDSS spectroscopy.

Comets found by	Imaging	In spectra	Notes
Dalcanton	1	0	Not in DR5
Visual	5	2	1 future target, 2 not in DR5
Accidental spectra	4	4	All found
Spectra check	2	2	All previous found +2 new ones
Total	12	8	1 future target and 3 not in DR5

scopic flux limit. SDSS should be able to reliably find comets with $r < 20$, while fainter comets become non-trivial to confirm by visual inspection. We utilize the eight comets with $r \leqslant 17.7$ (Petrosian), found using the spectra, as a control group to develop and test a robust method for selecting candidate comets with $r < 20$ from the imaging data alone.

2.5. The faint candidates

Five selection criteria based on cataloged parameters measured by the photometric pipeline were developed to significantly reduce the number of objects from the 215 million objects present in DR5. This sample pruning is needed to produce a reasonable number of candidates for visual inspection, as was done with the 6771 candidates pre-selected using spectroscopy. This selection algorithm must preserve the control set of eight comets which we assume is nearly complete[5] for $r \leqslant 17.7$ (Petrosian). The selection criteria are:

(1) Objects must be brighter than $r = 20$, to have a sufficient signal-to-noise ratio for reliable visual confirmation of their cometary nature in the imaging data.
(2) Objects must be resolved. These are active comets at small heliocentric distances, and thus their comae are resolved objects. Our requirement for a resolved object is that the difference between the psf and model *r* magnitudes, Δr, be greater than 0.2, a slightly less restrictive cut than the one used for morphological star–Galaxy classification by the Galaxy spectroscopic targeting algorithm ($\Delta r > 0.3$; Strauss et al., 2002).
(3) Objects must have a measured angular velocity greater than $v = 0.04$ deg/day. This limit corresponds to the angular motion of an object in a circular orbit at about 20 AU (roughly the orbit of Uranus). For comparison, main-belt asteroids observed at opposition typically have $v = 0.2$ deg/day (see Fig. 14 of Ivezić et al., 2001). The mean astrometric accuracy of the SDSS allows for an eight σ detection to correspond to $v = 0.025$ deg/day (Ivezić et al., 2001).
(4) The angular velocity should be significant when compared to its measurement error, and a limit of $v/\sigma_v > 4$ was chosen (see Fig. 6 of Ivezić et al., 2001).
(5) All eight of the control comets have at least one of three DEBLENDED flags set by the SDSS photometric pipeline. The three binary flags are: DEBLENDED_AS_MOVING, assigned to complex objects that the photometric pipeline identifies as having moved during the 5 min of imaging, DEBLENDED_AT_EDGE, assigned to larger, complex objects (typically larger than 1′) that were imaged at the edge of the detector, and DEBLENDED_DEGENERATE, which is assigned to complex objects where the photometric pipeline gave two or more valid deblending solutions. For more details see Section 4.4.3 of Stoughton et al. (2002). The final selection criterion requires that at least one of these three flags has been set.

In order to check that these selection criteria worked as intended, they were applied to the spectroscopic galaxies ($r \leqslant 17.7$ Petrosian), reducing that sample from 440,502 objects to just 2262, with no restrictions on spectral classification. Table 2 shows how the application of the five cuts achieve that result. These 2262 images were visually inspected and returned the same eight comets that had been found through examining the 6771 objects

Table 2
The initial criteria for selection of candidate comets applied to DR5 and the subset of spectroscopic galaxies. The selection cuts are applied sequentially.

Criteria	Selection	DR5 imaging	DR5 spectroscopic galaxies
DR5	None	Approx. 215 million	440,502
Bright	$r < 20$	69.9 million	440,502
Resolved	(psf-model) $r > 0.2$	18.6 million	440,502
Moving	$v > 0.04$ deg /day	1.6 million	6995
Significant	$v/\sigma_v > 4$	1 million	4244
Flag set	At least one flag set	157,996	2262

[5] Here "nearly complete" means that there are not more than one or two other comets with $r \leqslant 17.7$ (Petrosian) detected in DR5 images, but not recognized as comets.

morphologically selected as galaxies, but not matching Galaxy-type spectra. No new comets were found in this new set of 2262 candidates, demonstrating that the restriction to inspect only objects that had spectra inconsistent with Galaxy classification did not introduce any additional strong incompleteness to the sample.

Applying these five cuts to the full DR5 catalog reduces the 215 million object catalog to 157,996 objects (with $r < 20$). Fig. 3 compares the distributions of these 157,996 objects and comets from the control sample in diagrams constructed using the parameters utilized by the selection criteria. Out of these 157,996 objects, 106,291 have $17.7 < r < 20$, and may include additional comets that would have been below the magnitude limit for spectroscopic selection.

Objects that are candidate comets must be visually inspected in order to ascertain if they are truly comets. While the initial five cuts dramatically reduce the size of the candidate objects by over a factor of 1000, a sample of ~150,000 objects is still too large to effectively examine by eye, and tighter constraints must be enforced to further decrease the sample size. Examining the measured properties of the known comets shows several properties that can be used to further reduce the sample size: (1) the initial constraints placed on Δr and velocity seem too generous as discussed below and (2) the color distribution of the control comets is remarkably narrow (discussed in more detail in Sections 2.7 and 3.4). This suggests two additional cuts: (1) impose tighter constraints on Δr and minimum velocity, or (2) restrict the search to objects whose colors match the narrow range of colors exhibited by the control comets.

2.6. Velocity–size selection

Comets in the control sample and all other serendipitously found comets have an angular velocity larger than $v = 0.04$ deg/day, with a median value of $v = 0.12$ deg/day. Fig. 3 shows the relative "buffer" room between the lower angular velocity limit and the motion of the majority of the comets. The comets are also significantly more resolved than what the lower limit of $\Delta r = 0.2$ indicates. The most point-source like has $\Delta r = 1.19$, and the control comets as a group have a median $\Delta r = 1.92$. Therefore more restrictive cuts were made: $v > 0.1$ deg/day and $\Delta r > 1$. Out of the eight comets from the control sample, six pass these more restrictive criteria. The two comets that fail both had measured angular velocities less than 0.1 deg/day (0.04 and 0.09 deg/day, respectively). Enforcing these two restrictions reduced the $r < 20$ sample of 159,996 by a factor of four to 43,005 objects.

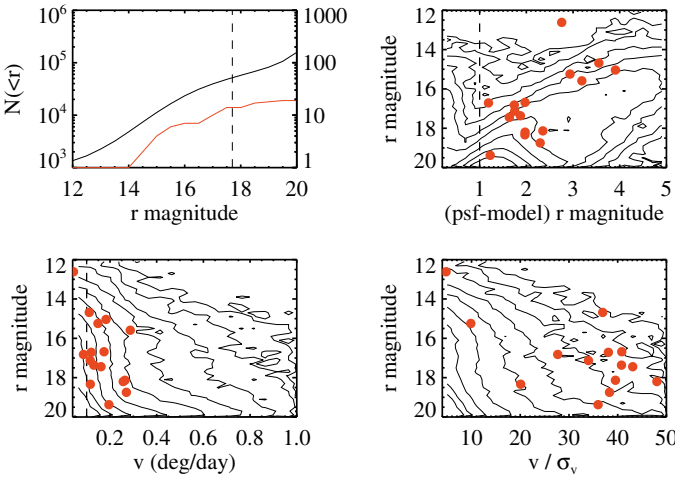

Fig. 3. Top left: Cumulative r-band magnitude distribution of the 157,996 candidate objects (black line, left axis), and the SDSS comets (red line, right axis). The dashed line at $r = 17.77$ shows the limit of SDSS spectroscopy. The other three plots show the distribution of measured properties used in the selection criteria for the 157,996 candidate objects (contours) and the control comets from spectroscopy (symbols). The vertical dashed lines in the top right and bottom left panels show the more restrictive size and velocity cuts discussed in Section 2.6. (For interpretation of the references to colour in this figure legend, the reader is referred to the web version of this article.)

These 43,005 objects were visually inspected and 16 comets were identified. In addition to the 6 from the control sample, 10 additional comets were identified. Two of the 10 additional comets also had $r < 17.7$ (Petrosian). These two objects were targeted for spectroscopic follow-up, but the spectra had not been taken by the time of DR5's release (and thus do not imply an incompleteness of the control sample). The eight remaining new detections are all fainter ($r > 17.7$ Petrosian) than the spectroscopic limit.

2.7. Color selection

The comets detected by SDSS have a narrow distribution of g–r, r–i and i–z colors. Table 3 and Fig. 4 illustrate this trend, which is discussed in detail in Section 3.4. A three-dimensional color cut was then applied, preserving the majority of known comets, and reducing the size of the candidate sample considerably. We required that $g - r = 0.57 \pm 0.25$, $r - i = 0.23 \pm 0.2$ and $i - z = 0.08 \pm 0.4$. Six out of the eight control comets satisfy these constraints. One of the control comets that fails these color cuts also failed the size–velocity cuts because of its low angular velocity ($v = 0.04$ deg/day). Fig. 5 shows these cuts in color–color space. Applying these color cuts to the 157,996 candidates left 16,254 color-selected candidates. Those objects were visually inspected, and 14 comets were identified.

When both the selection based on color described here, and the more restrictive velocity and size restrictions (Section 2.6) are enforced together on the 157,996 candidate objects ($r < 20$), 4510 objects pass the cuts, containing 13 comets. The one comet selected using the color method that was not also selected by the velocity and size method had a measured angular velocity of $v = 0.09$ deg/day, below the more restrictive limit of 0.1 deg/day.

Utilizing these methods a total of 18 images of 16 active comets were positively identified in DR5. Two comets were imaged twice. Including comets that were identified in older runs, now superseded by the more recent imagery, a total of 22 images of 19 active comets have been found. Fig. 6 shows g, r, i color composites of 20 of these images.

3. Results

Here, we present two initial results based on the sample of 16 active comets (18 detections) found in DR5. SDSS is being treated as a single snap shot of the sky, so to avoid bias we have only used the first observation of the multiply observed comets. The first result is the distribution of active comets with respect to magnitude and to ecliptic latitude. The second result is the evidence for an extremely narrow distribution of the SDSS colors (u–g, g–r, r–i, i–z) of active comets.[6]

3.1. Incompleteness

Using the sample of comets found in DR5 allows placement of lower limits on the distribution of active comets as a function of their magnitude and position on the sky. The major contribution to the incompleteness of the sample presented here is that the comets must have been "identified" by two different sources. First, the comets must have been properly identified and processed by the SDSS software. As mentioned previously, some extended ob-

[6] The rms scatter of the comet colors is a factor of 3–4 times smaller than the color cuts discussed in Section 2.7.

Table 3
Properties of the active comets identified in SDSS. The table lists r band magnitude, SDSS colors, measured velocity, and the difference between the model and psf magnitudes (Δr). The geocentric distance (Δ) and the heliocentric distance (R) in AU at the time of the SDSS observation are also cited, except for the two comets designated by *Unk1* and *Unk2* which were not matched to any known object (comets or asteroids). The designations (first) and (second) refer to the chronological order of comets with multiple detections.

Comet	r	$u-g$	$g-r$	$r-i$	$i-z$	deg/day	Δr	Δ	R
30P Reinmuth	14.85	1.60	0.57	0.32	0.19	0.42	2.2	1.46	1.88
46P/Wirtiran[a]	18.84	−1.25	3.39	0.22	0.12	0.32	1.63	1.64	2.60
50P/Arend	18.13	1.72	0.57	0.08	0.27	0.26	2.35	2.57	2.81
62P/Tsuchinshan	15.04	1.27	0.45	0.18	0.07	0.18	3.91	0.95	1.90
65P/Gunn (first)	17.13	1.68	0.58	0.21	0.08	0.12	1.75	3.55	4.34
65P/Gunn (second)	17.15	1.57	0.55	0.21	0.09	0.11	1.9	3.56	4.34
67P/Churyumov-Gerasimenko	14.29	1.83	0.68	0.24	0.06	0.29	3.15	1.59	1.84
69P/Taylor	15.59	1.51	0.60	0.25	0.06	0.29	3.19	1.13	1.95
70P/Kojima	16.68	1.47	0.64	0.23	0.21	0.17	1.97	1.63	2.59
C/1999 F2 Dalcanton	15.18	1.76	0.62	0.31	−0.18	0.06	2.29	4.34	5.00
C/2000 K2	16.82	1.55	0.55	0.22	0.10	0.09	1.74	6.00	5.25
C/2000 QJ46 (first)	17.44	1.55	0.57	0.23	0.12	0.16	1.64	1.16	2.17
C/2000 QJ46 (second)	19.39	1.04	0.56	0.41	0.09	0.18	1.47	3.32	3.66
C/2000 SV74	14.68	1.66	0.52	0.21	0.04	0.11	3.55	4.02	4.38
C/2000 Y2 Skiff	16.71	1.58	0.55	0.18	0.09	0.12	1.19	1.82	2.79
C/2001 RX14[a]	12.62	1.24	1.43	0.10	−0.33	0.04	2.76	1.62	2.10
C/2002 O7 (first)	19.37	1.35	0.58	0.14	−0.21	0.20	1.23	5.65	5.89
C/2002 O7 (second)[a]	15.24	0.60	2.07	−0.27	−0.71	0.15	2.94	2.50	3.04
C/2002 T5	18.33	1.52	0.66	0.23	0.09	0.12	1.97	4.35	5.00
P/1999 V1 Catalina	17.36	1.73	0.58	0.23	0.09	0.13	1.87	2.16	3.10
Unk1	18.20	2.71	0.48	0.36	0.24	0.26	1.97	–	–
Unk2[a]	18.75	1.86	0.98	0.14	−1.49	0.27	2.30	–	–
Median color		1.62	0.57	0.24	0.08				
Std. dev.		0.34	0.06	0.08	0.12				

[a] Comets suffer from significant deblending issues, and were not included in the calculation of median and standard deviation for the sample color distributions.

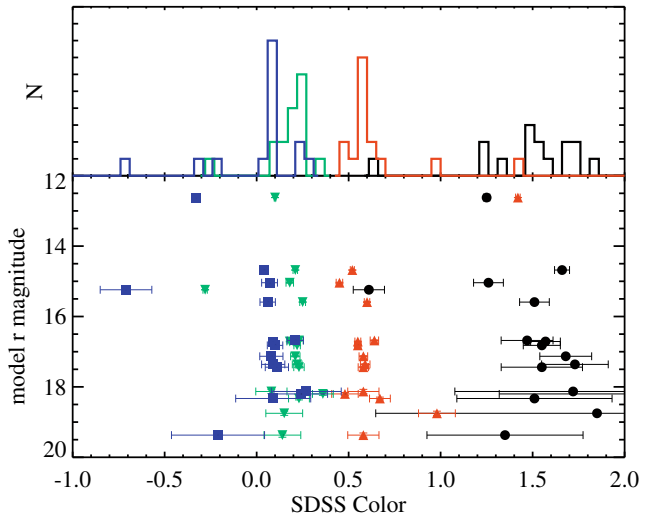

Fig. 4. The color–magnitude distribution of the DR5 comets with 2 − σ error bars as determined by the photometric pipeline. The plotted symbols are: ◯ $u-g$ (black), △ $g-r$ (red), ▽ $r-i$ (green), and □ $i-z$ (blue). Plotted above is the histogram of the color distribution. The large outliers are comets with significant deblending errors as discussed in Section 3.4. (For interpretation of the references to colour in this figure legend, the reader is referred to the web version of this article.)

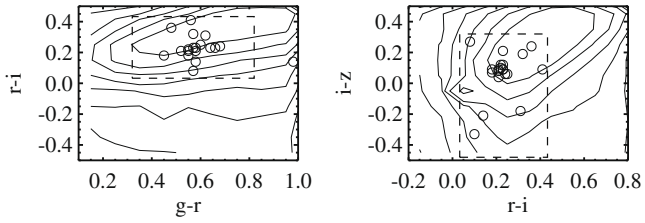

Fig. 5. The dashed-line rectangles show the cuts made in color–color space, shown on top of contours of the 157,996 candidates. Comets are shown by open circles.

jects may be deblended to the point where the reported properties no longer fall within the bounds of the cuts used in the given selection criteria. This will be shown to be the case for the comets that failed the color cuts in Section 3.4.

Second, the comets in DR5 must be identified and confirmed by eye. Two incompleteness issues arise with respect to this. First, the field containing the comet must be present within the DR5 database, as well as the corresponding image stamp. The design of the SDSS imaging survey allows for a small area of overlap between runs adjacent on the sky. If a comet is in one of these "overlap" regions, it is possible for the image of the section of the sky containing the comet to actually belong to a newer run from a different epoch (when the comet was not at that location). For example, the comets found in earlier data releases such as C/1999 F2 Dalcanton are no longer present in DR5. The second source of incompleteness is endemic to visual inspection: it is possible to miss a few comets, especially at the faintest magnitudes. As r nears 20 the cometary nature of the comet, easily identifiable at brighter magnitudes becomes much more difficult to discern.

3.1.1. Tests of incompleteness

In order to check the incompleteness, we examined a list of currently observable Jupiter family comet orbits maintained by the MPC[7] and calculated, using codes described by Jurić et al., 2002, where their orbits intersected an SDSS field in space and time. These matches were then visually inspected to see if a comet was actually there. Nine comets were matched in DR5 this way. Four of these comets had been found by the selection process detailed in this work. Another four had $r > 20$, fainter than the limiting magnitude of the study. The one remaining comet was missed as it was overlapping with a moderately bright star, resulting in an object whose velocity and deblending flags excluded it from the main selection criteria. The implied sample completeness based on this test is 80% (4 out of 5 possible detections are recovered by catalog-based search).

[7] This list contains comets that have been recently observed, and thus is generally restricted to comets brighter than $v = 21$ and to solar elongations greater than 30°.

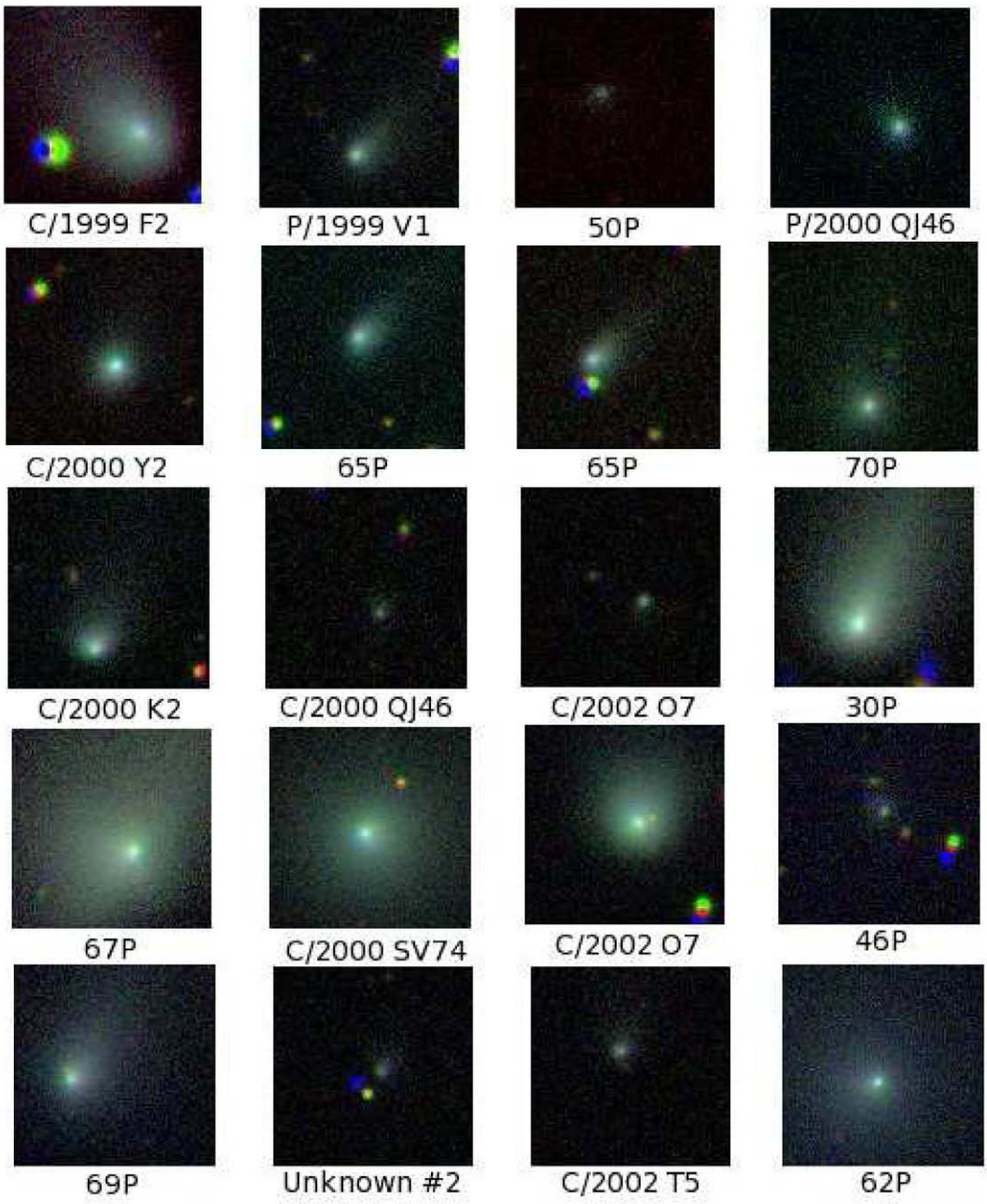

Fig. 6. An image collage of 20 images of 17 comets discussed in the paper. The color images are RGB color composites of the *g*, *r* and *i* filters of the comets. All image stamps are approximately $40'' \times 40''$. These RGB images were made by registering the images to the motion of the comets, rather than the position of the background stars. (For interpretation of the references to colour in this figure legend, the reader is referred to the web version of this article.)

3.2. Magnitude distribution of active comets

The sample of comets can be divided into two groups based on completeness. The bright comets with $r \leqslant 18$ represent a much more complete sample than fainter comets – their transient nature is confirmed with a second epoch of observations (the spectroscopic survey), and they are bright enough to make visual identification robust.

Making simple linear fits to the cumulative number of comets as a function of magnitude allows an estimation of how many comets could be expected to be found at $r < 20$, as used here, and at the much fainter magnitudes achievable with the next generation of large-scale survey telescopes. Fig. 7 and Tables 4 and 5 detail these fits to the distribution found in this study. Taking the range of values from the fits we find estimates of between 100 and 260 active comets with $r < 20$, and between 260 and 2860 active comets with $r < 24$ on the whole sky at any time. The two estimates extrapolate from the faint ($r > 18$) and bright ($r < 18$) samples. These estimates are affected not just by incompleteness, but also the unknown nature of activity levels and timescales for extremely small cometary nuclei, the true size scale for cometary nuclei, and the non-uniform distribution of comets across ecliptic latitude.

3.3. Ecliptic latitude distribution of active comets

SDSS does not cover the full range of ecliptic latitude on the sky, seen in Fig. 1. The main survey does not sample below approximately $\beta = -20^\circ$ (although the Southern Survey does extend down to $\beta = -27^\circ$ for a very limited region of the sky), and the exact cov-

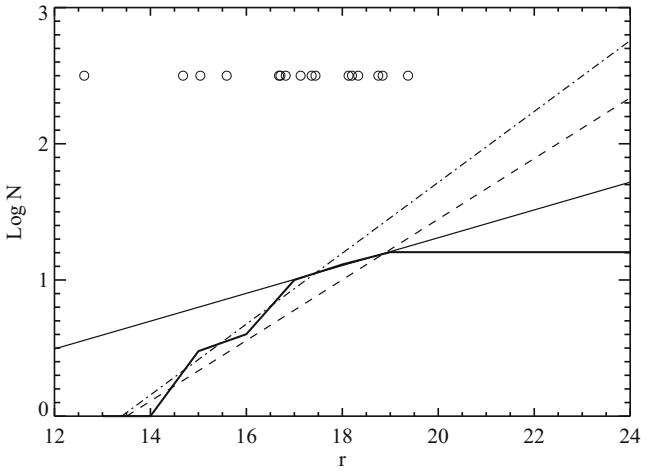

Fig. 7. Log of the cumulative number of comets found in DR5 with respect to r magnitude (solid line). Three other lines represent fits to (dashed) the total ($r < 20$) magnitude range, (dash-dot) the bright ($r < 18$) range, and (dash-triple dot) the faint ($r > 18$) range. The actual comet magnitudes are represented by open circles above the plot.

Table 4
Expected number of comets at both 20th and 24th magnitudes, for a 1/5 sky survey (like SDSS DR5), and for the whole sky. These estimates are extrapolated from the SDSS counts (cf. Fig. 7).

Fit	$r < 20$ 1/5 sky	$r < 20$ all sky	$r < 24$ 1/5 sky	$r < 24$ all sky
Bright: $r < 18$	52	260	572	2860
All: $r < 20$	28	140	218	1090
Dim: $r > 18$ and $r < 20$	20	100	52	260

Table 5
Surface brightness profile fits of the comets to $m = C - 5log(\Theta)$ in all five SDSS filters with standard deviation of the data around the median. These are based on the magnitude (m) and 50% Petrosian radius (Θ) of the comets and is shown in Figs. 16 and 15.

Filter	Fit constant (C)
u	22.64 ± 1.43
g	21.17 ± 0.88
r	20.19 ± 0.74
i	20.04 ± 0.73
z	19.97 ± 0.98

erage above that limit varies with ecliptic longitude. Fig. 8 demonstrates that within the known ecliptic latitude bounds of SDSS, our sample of comets spans the range of latitudes and heliocentric distances seen a single-night "snapshot" of currently observable comets maintained by the MPC.

Fig 9 illustrates the absolute ecliptic latitude distribution of the 306,751 (9×13 arc min^2) fields in DR5, the 159,996 candidate comets, and the populations of both the asteroids from MOC3 and the 16 comets found in DR5. Both the asteroid and comet populations are concentrated within low ($\beta < 25^\circ$) ecliptic latitudes, as expected for the main-belt asteroids and JFCs. Three comets were found at higher ecliptic latitudes, consistent with a second population of higher inclination comets (the LPCs). All three of the high β comets in DR5 were positively identified as known LPCs by the Minor Planet Center.

These distributions were corrected for the solid angle at a given ecliptic latitude (β) on the sky and for the distribution of DR5 observations with respect to β (Fig. 10). The cumulative histograms for the asteroid population reaches 90% by $\beta \sim 25^\circ$. The JFC component of the comets shows a similar trend, but because the comets also contain a second population (LPCs) there is evidence of a break in the distribution here, as the comet population transitions from one dominated by JFCs at low β to one dominated by LPCs at higher β.

3.4. SDSS colors of active comets

As discussed in Section 2.7, the SDSS-detected comets show a very narrow color distribution as summarized in Table 3. For example, the root-mean-square scatter for $g - r$ is only 0.06 mag, only marginally larger than the expected measurement errors (about 0.02 mag per band for point sources, and larger for resolved sources). This narrow distribution is 3–4 times narrower than the color cuts applied in Section 2.7. Four comets significantly deviate (>0.8 mag) from the median colors ($g - r = 0.57$, $r - i = 0.23$, and $i - z = 0.08$), but all four have significant deblending errors. Typically, the coma of the comet is separated into multiple objects by

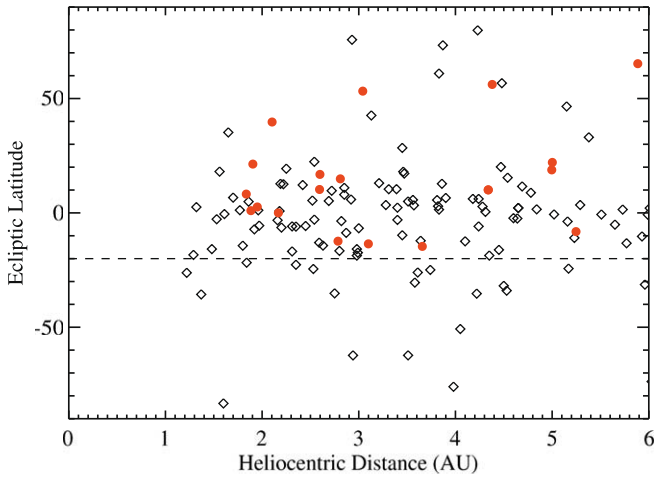

Fig. 8. The distribution of a single night "snapshot" of comets (from the MPC list of currently observable comets) in open diamonds, and the SDSS comet sample plotted in red circles. The dashed line at $\beta = -20^\circ$ represents the approximate lower limit of DR5, although the Southern Survey does extend to $\beta = -27^\circ$ for a small portion of the sky. (For interpretation of the references to colour in this figure legend, the reader is referred to the web version of this article.)

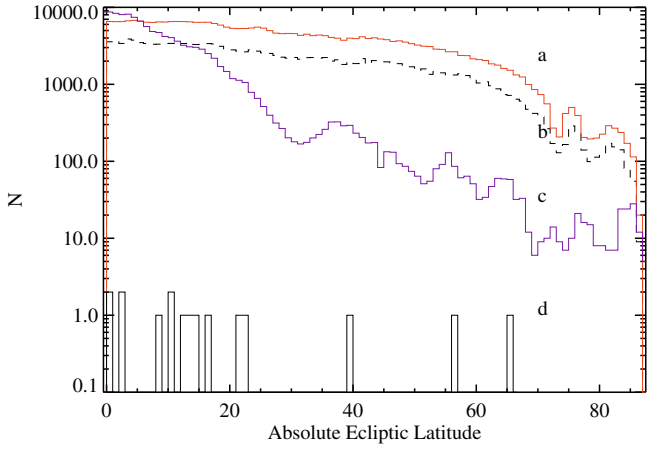

Fig. 9. The distribution of: (a) all DR5 fields, (b) the 157,996 candidate comets, (c) the asteroids in MOC3, and (d) the 16 DR5 comets with respect to absolute ecliptic latitude. Two populations of comets can be seen. All known Jupiter family comets in the sample can be found at low β, and the three comets observed at high β were identified as long period comets by the Minor Planet Center.

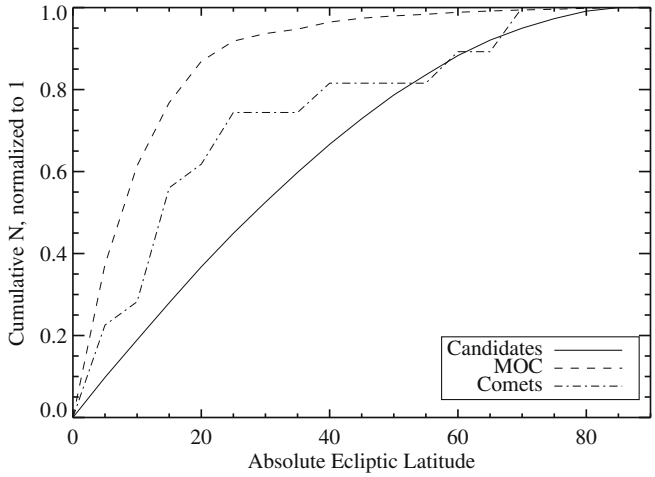

Fig. 10. The absolute ecliptic latitude distributions from Fig. 9, corrected for the latitude distribution of DR5 fields and the differential solid angle at a given ecliptic latitude (β). Unlike the asteroids in the MOC, the comet population demonstrates a change of slope at around $\beta = 25$ showing evidence for two comet populations.

the photometric pipeline. The resulting photometry of the comet is thus missing significant flux in at least one filter. Fig. 11 illustrates one family of deblended images for a comet that failed the color selection. Even comets that marginally deviated from the median colors showed at least some deblending errors. For example, C/1999 F2 Dalcanton deviates from the median color in each of $g - r$, $r - i$, and $i - z$ by about 0.1 mag. In the case of this comet, the coma was properly deblended, but the tail was not.

Despite deblending errors, enough of the comets were treated properly by the pipeline to show that their colors are similar to colors reported by other observers. Transforming the SDSS colors into synthetic *BVRI*, using relations from Ivezić et al., 2007, the colors of the comets in this study fall within the range presented by Lowry et al. (1999, 2001, 2003). Fig. 12 shows the comparison between the comets studied by Lowry et al. and the synthetic *BVRI* derived for the sample of SDSS comets.

The SDSS colors of comets are compared to those of the asteroids in the SDSS Moving Object Catalog in Fig. 13. To elucidate a more detailed comparison between the colors of active comets and typical colors for other Solar System small bodies, the reflectance (normalized to the *r* band) for various sub-populations of the main-belt asteroids and the Trojans of Jupiter are shown in Fig. 14. We find that the reflectance of active comets most closely matches that of the jovian Trojans (Szabó et al., 2007). This result is surprising, since Trojans have solid surfaces, while these comets have a diffuse coma. The similarity between active comets and jo-

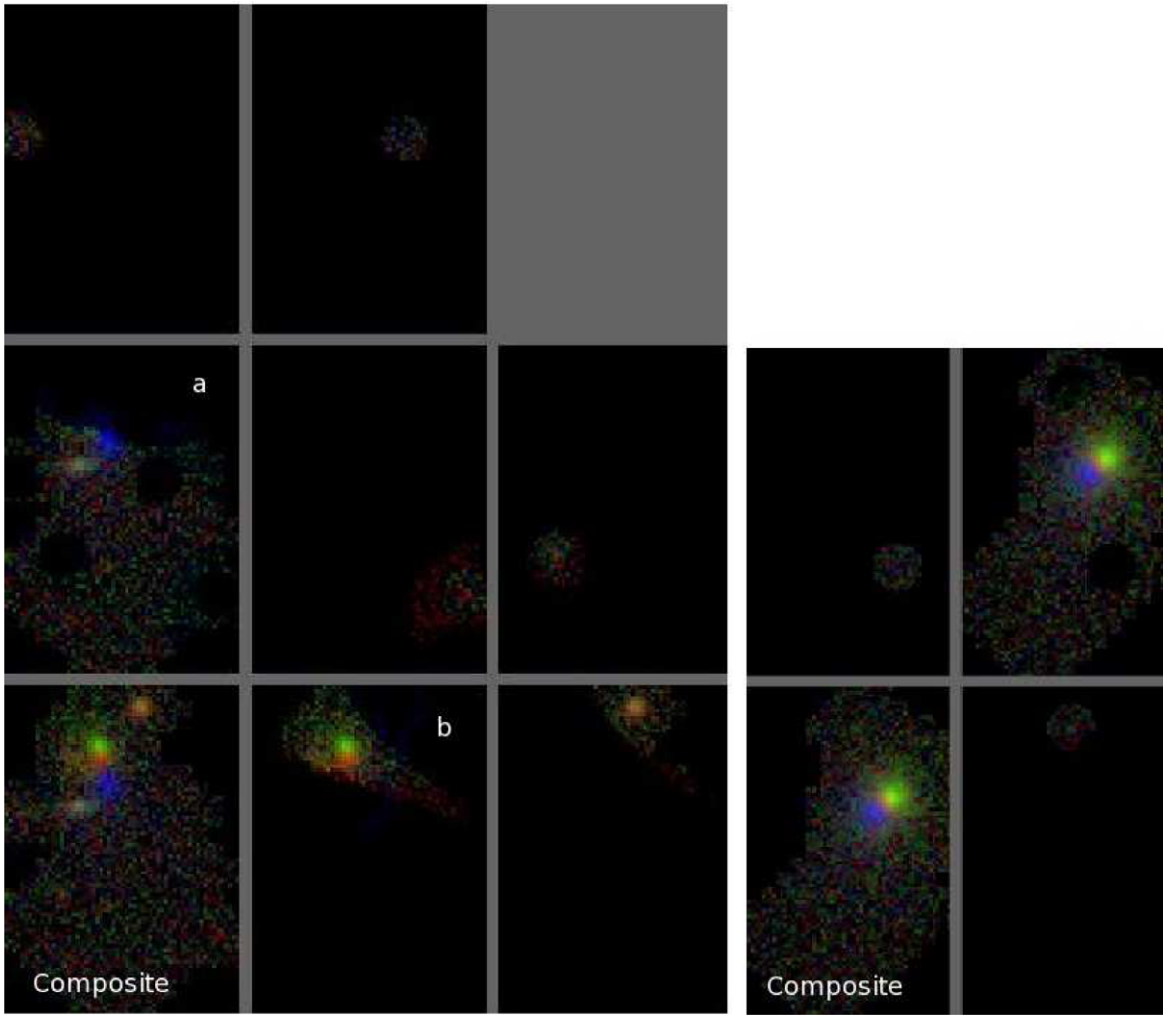

Fig. 11. Left: an example of the badly deblended Comet 46P/Wirtiran. The colors represent the *g*, *r* and *i* filters. The lower left image is the composite (*gri*) image, and the others are the separately treated objects that the deblender has divided the original image into. Notice that the head of the comet has been deblended into two separate objects in the squares labeled **a** and **b**. Right: a similar figure showing the first observation of comet C/2000 QJ46 (LINEAR) which was not pulled apart in the deblending process. (For interpretation of the references to colour in this figure legend, the reader is referred to the web version of this article.)

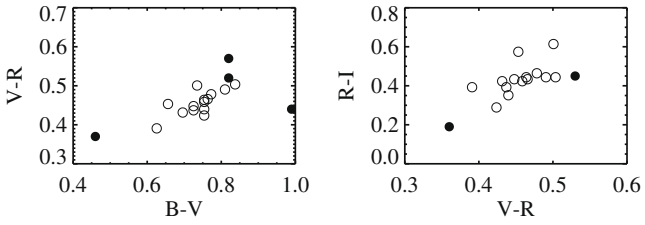

Fig. 12. The colors of the SDSS comets transformed into *BVRI* (open circles) and compared to the colors of active comets cited by Lowry et al. (1999), Lowry and Fitzsimmons (2001), and Lowry et al. (2003) (filled circles). The transformation from SDSS colors to *BVRI* is given by Ivezić et al. (2007).

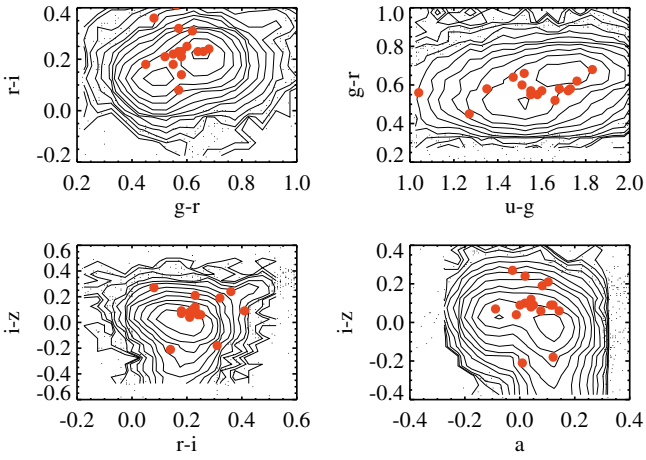

Fig. 13. The color distribution of comets (filled circles) vs. the colors of the asteroids listed in the MOC. "*a*" is the principle component color in the MOC defined as $a = 0.89\ (g-r) + 0.45\ (r-i) - 0.57$ (see Ivezić et al., 2001). (For interpretation of the references to colour in this figure legend, the reader is referred to the web version of this article.)

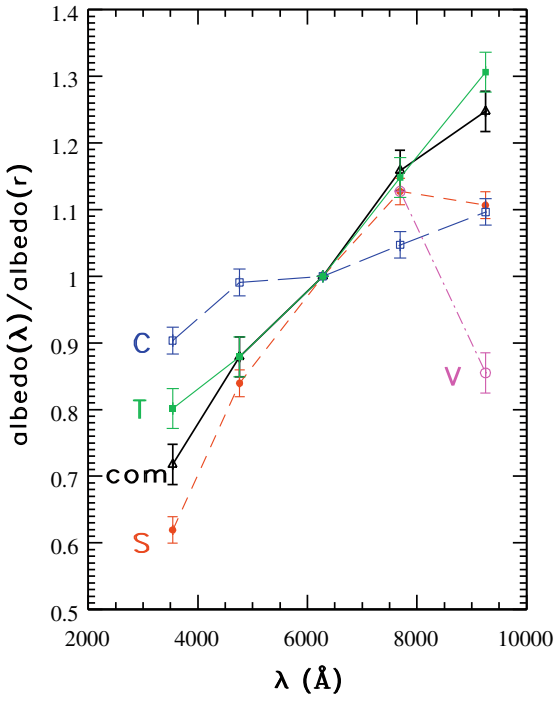

Fig. 14. A comparison of the relative reflectance for comets (black triangles), the relative albedo for jovian Trojans (green filled squares) and the three dominant main-belt color types (C type: open blue squares; S type: red dots; V type: magenta open circle; the V type differs from the S type only at the longest displayed wavelength) normalized to the *r* band. The errors are dominated by the systematic absolute uncertainties in the SDSS photometric calibration. Because the same systematic uncertainty applies to all curves, their differences are highly significant (the relative positions of data points are accurate to about 0.01). The albedo curve for active comets is more similar to the albedo curve of jovian Trojans than to albedo curves for main-belt asteroids, despite the clearly different origins of the light (coma vs. solid body). (For interpretation of the references to colour in this figure legend, the reader is referred to the web version of this article.)

vian Trojans was also noted in 5.2—38 μm observations (Emery et al., 2006), and may have implications for surface conditions of Trojans, but a detailed analysis of this color similarity is beyond the scope of this work.

3.5. Size–magnitude relationship of active comets in SDSS

We investigated the surface brightness of the SDSS comets, since it could serve as a useful discriminate between galaxies and comets – the light from comets has a very different physical origin than the light from galaxies. We use the magnitude and the 50% Petrosian radius (a measurement of effective angular size) to derive and compare the surface brightness distribution for the confirmed comets and the full candidate sample in each of the five SDSS filters in Figs. 15 and 16. Lines of constant surface brightness have been over-plotted for comparison.

Even without correcting for deblending problems, the comets do show a simple relationship between magnitude and size. The magnitude of an extended object should be linearly related to $-2.5log(\Sigma\Theta^2)$, where Σ is a surface brightness, and Θ the angular size. Assuming constant surface brightness, there should exist a relation of $m = C - 5log(\Theta)$. We find that our sample of comets is best fit by a relation of $m = 20.19 - 5log(\Theta)$ in the SDSS *r* band, with Θ expressed in arc seconds.

Hence, it turns out that comets in our sample do have a fairly narrow surface brightness distribution, with a root-mean-square scatter around the best-fit *m* vs. Θ relation of only 0.8 mag in the SDSS *r* band. However, the value of their median surface brightness is similar to typical surface brightness observed for galaxies, and therefore surface brightness is not a good comet–Galaxy separator.

Another potential separator of comets and galaxies is the *shape* of their surface brightness profiles. We quantify this shape using the concentration index (the ratio of 90% and 50% Petrosian radii), and show its distribution in Fig. 17 for the comets and the candidates. While the distribution of this ratio for confirmed comets is different from that for the whole candidate sample, it is still not as robust a selection parameter compared with the previously discussed cuts on color, size and velocity, and does not even reduce the candidate sample by a factor of 2. It is interesting that the distribution of the Petrosian radius ratio for the candidate sample is skewed towards smaller values (<1.7), compared to the expected distribution for galaxies, which fall off much more sharply at <1.7. This investigation showed that the candidate sample also includes a substantial number of saturated stars (cf. Fig 18).

What is noticed in Fig. 17 is that the distribution of the concentration index for the observed comets is not significantly different than that of the expected concentration indices for the Galaxy fit models used by the SDSS photometric pipeline. Fig. 19 shows the measured surface brightness profile for the observed Comet 30P Reinmuth. The comet's profile is compared to the expected profile of a steady-state coma, both with and without taking radiation pressure into account (see Jewitt and Meech, 1987). We find that the surface brightness profile is only slightly steeper than expected for a radiation affected steady-state coma. Fig. 19 shows that even though the comet's profile is not, in nature, like that of a Galaxy the model fits used by SDSS to generate the model magnitudes do not

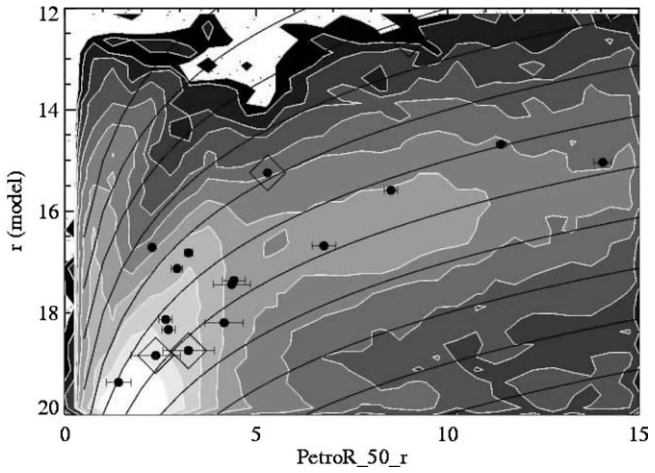

Fig. 15. The relationship between the magnitude of the observed comets (filled circles, with those suffering from major deblending errors surrounded by open diamonds) and their angular radius, Θ, taken as their measured 50% Petrosian radius (with reported 2σ error bars) in the r band. The lines represent lines of constant surface brightness, $r = C - 5log(\Theta)$ for constant values of C ranging from 15 to 25. The best fit for the comets is $C = 20.19 \pm 0.74$ (see Table 5).

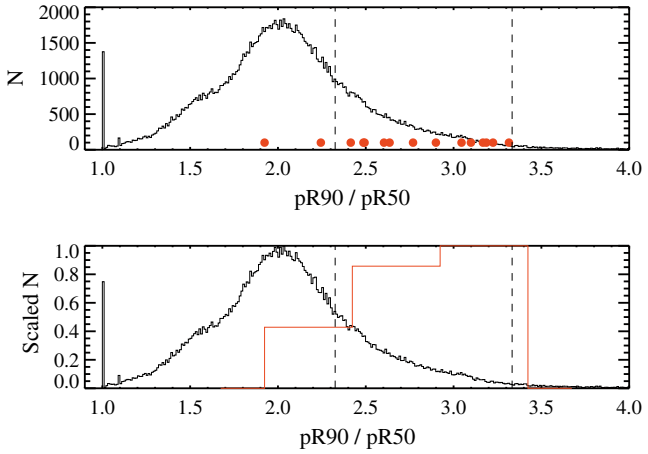

Fig. 17. Histogram of the ratio of the 90–50% Petrosian radius (pR90 and pR50) measured for each of the 157,996 DR5 candidates. The DR5 comets are shown as red dots. Two dashed vertical lines represent what would be expected from the two Galaxy model fits (exponential and de Vaucouleurs). The singular spike at pR90/pR50 = 1 is from diffraction spikes. (For interpretation of the references to colour in this figure legend, the reader is referred to the web version of this article.)

significantly deviate from the measured surface brightness profile. In the case of 30P Reinmuth the de Vaucouleurs profile is a better fit; expected as the SDSS concentration index for this comet was measured to be 3.13, closer to the concentration index of a pure de Vaucouleurs profile $\sim$(3.3), than to an exponential profile $\sim$(2.3).

4. Discussion

We have searched for active comets in the SDSS data, which provides accurately calibrated and measured multi-wavelength data and, since the search is unbiased above the faint flux and angular resolution limits, a measure of the distribution of active comets in color, magnitude and location on the sky.

In this work, we used a training sample of comets serendipitously detected by SDSS, and developed well-controlled selection criteria to reduce the number of plausible comet candidates to a sample size that could be visually inspected. After the visual inspection that rejected false positives, the total sample of SDSS comets presented here includes 19 objects.

In addition to providing information about individual objects, the well-understood selection effects enable us to study population statistics. We estimated the magnitude distribution down to $r \sim 18$, and found evidence for two populations in the sample ecliptic

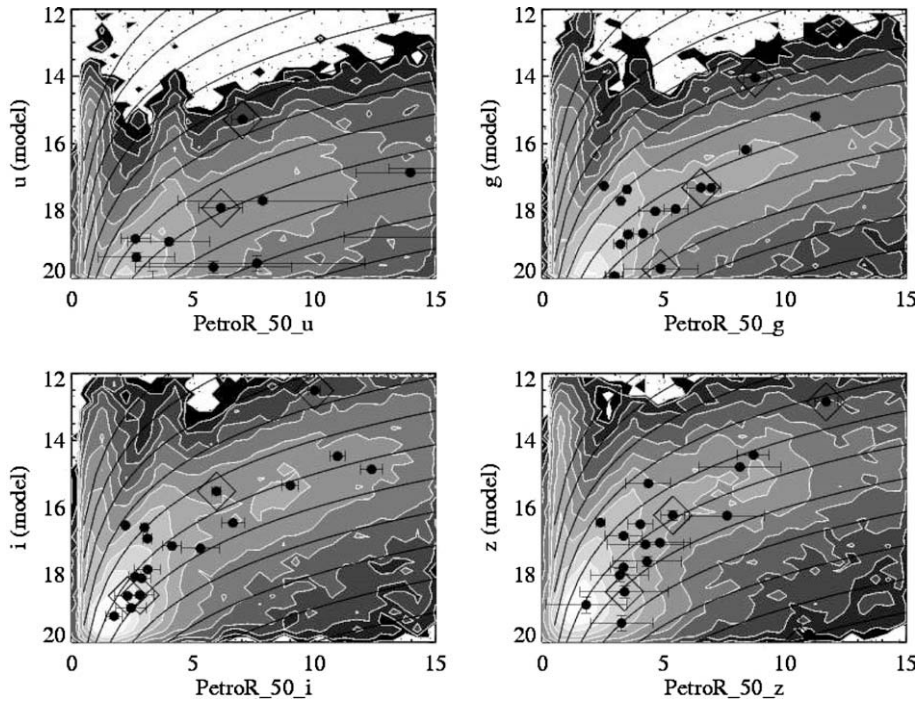

Fig. 16. Analogous to Fig. 15, except for u, g, r and z bands. Table 5 summarizes the fits for all five bands.

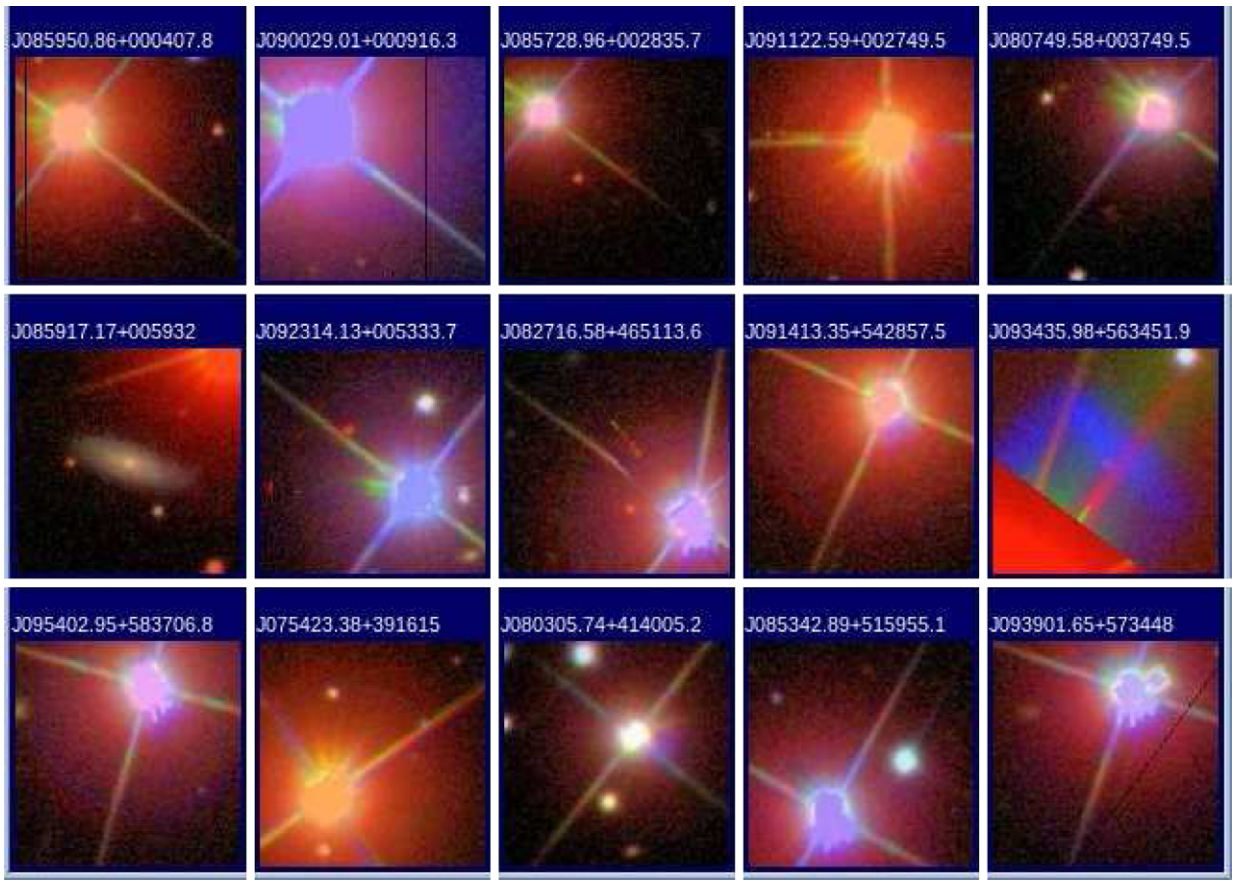

Fig. 18. Examples of candidate objects with 8 < PetroR50 < 10 and $16 < r < 17$, a region of background over-density in Fig. 15. These do not look significantly different than those objects that populate the over-density feature with 1 < PetroR50 < 2, and $15 < r < 16$. While these brighter false positives tend to be diffraction spikes the fainter candidate objects are generally faint or low surface brightness galaxies as well as imaging "ghosts" from a bright source out of the frame. All image stamps are $24'' \times 24''$ downloaded as jpg's from the SDSS sky server.

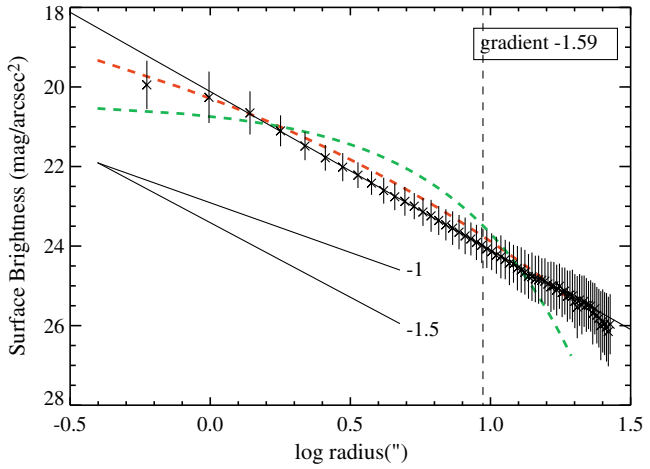

Fig. 19. The *r*-band surface brightness profile of the Comet 30P Reinmuth. The best fit gradient of −1.59 is over-plotted on the data. The plotted gradients of −1 and −1.5, represent the predicted surface brightness profile for a steady-state models of the coma. The steeper gradient accounts for radiation pressure. Dashed curves show the model fits used by SDSS, a de Vaucouleurs profile in red, and an exponential profile in green. Of the two the de Vaucouleurs is the better fit. The vertical dashed line marks a physical radius of 10^5 kilometers. (For interpretation of the references to colour in this figure legend, the reader is referred to the web version of this article.)

latitude distribution as can be seen in the changing slope for the comet population in Fig. 10. Perhaps the most surprising result is the extremely narrow color distribution for comets (e.g. root-mean-square scatter of only ∼0.06 mag for the $g - r$ color). No aspect of the data analysis should artificially produce such a narrow color distribution. In s sequel paper, we will present results based on custom photometry optimized for comets. The cometary colors were found to be close to those of jovian Trojan asteroids, but quite different from those of main-belt asteroids. This similarity may hold clues about the possible surface conditions, and nature of, the Trojans.

4.1. Future large scale surveys

The analysis and conclusions presented here are relevant for upcoming large-scale deep optical surveys such as the Dark Energy Survey (Flaugher, 2008), Pan-STARRS (Kaiser et al., 2002) and the Large Synoptic Survey Telescope (Ivezić et al. 2008, LSST hereafter). The results of Section 3.2 can be used to estimate the number of comets that these surveys might discover. For example, assuming LSST's depth for a single observation to $r = 24$, we estimate that at any given time LSST should be able to detect about 500 active comets, though this estimate is uncertain by at least a factor of two due to extrapolation of the SDSS results to much fainter magnitudes. An additional complication is the unknown nature and duration of the cometary activity for very small bodies as well as the size distribution of nuclei, all problems that these future surveys will help address.

The samples obtained by these upcoming deep multi-epoch surveys will include multiple-epoch observations of the same objects. We used magnitude predictions from the JPL's Horizons database to roughly estimate how long would an object be observable (see Fig. 20). These magnitude predictions imply that some fraction of comets would be bright enough to be detectable by

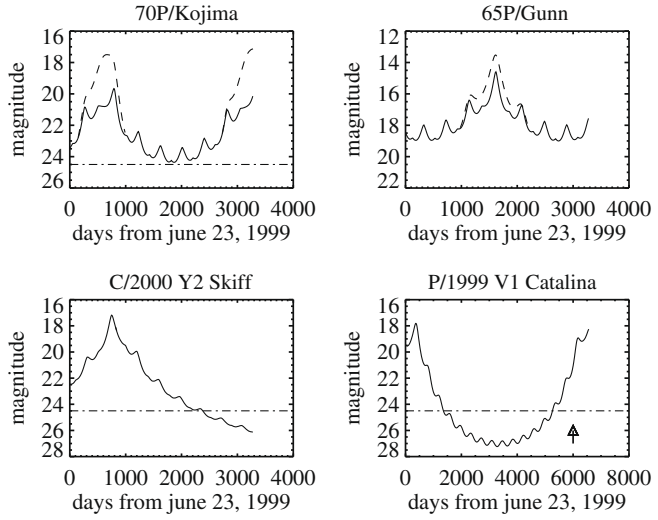

Fig. 20. The predicted visual magnitude of four comets from this study over at least a portion of their orbits. The comet will be inactive (asteroidal in appearance) for most of its orbit, and the solid lines represent the predicted nuclear magnitude of the comet. The rising dashed lines show the predicted magnitude the comet will reach while active during that part of it orbit. All magnitudes were predicted by the Jet Propulsion Laboratory's Horizons database (http://ssd.jpl.nasa.gov/?horizons). The horizontal dash-dot line at 24.5th magnitude represents the limiting magnitude for a single observation with LSST, which should see first light at around day 6000 (2015). As can be seen for both comets Kojima and Gunn, LSST will be able to detect these comets at all observable points in their orbits, and even for very long period comets like Skiff LSST will be able to greatly enhance the period of observable time for these objects.

LSST at any point in their orbits (dependent on the actual size distribution of cometary nuclei). Assuming conservatively that a comet would be observable only for about 6 months (and ignoring the fact that periodic comets would sometimes "come back"), we estimate that the LSST sample collected during a 10-year long survey would include about 10,000 objects observed on average about 50 times; for some, the LSST data set could include as many as 1000 detections. This volume of observations will allow for the detailed study of time evolution of cometary activity while active and establish light curves for the nuclei while inactive. In addition these upcoming surveys will obtain repeated observations for which image differencing techniques could find moving resolved sources, allowing for detailed measurement of their profiles without contamination by background stars and galaxies.

Acknowledgments

Funding for the SDSS and SDSS-II has been provided by the Alfred P. Sloan Foundation, the Participating Institutions, the National Science Foundation, the US Department of Energy, the National Aeronautics and Space Administration, the Japanese Monbukagakusho, the Max Planck Society, and the Higher Education Funding Council for England. The SDSS Web Site is http://www.sdss.org/.

The SDSS is managed by the Astrophysical Research Consortium for the Participating Institutions. The Participating Institutions are the American Museum of Natural History, Astrophysical Institute Potsdam, University of Basel, University of Cambridge, Case Western Reserve University, University of Chicago, Drexel University, Fermilab, the Institute for Advanced Study, the Japan Participation Group, Johns Hopkins University, the Joint Institute for Nuclear Astrophysics, the Kavli Institute for Particle Astrophysics and Cosmology, the Korean Scientist Group, the Chinese Academy of Sciences (LAMOST), Los Alamos National Laboratory, the Max-Planck-Institute for Astronomy (MPIA), the Max-Planck-Institute for Astrophysics (MPA), New Mexico State University, Ohio State University, University of Pittsburgh, University of Portsmouth, Princeton University, the United States Naval Observatory, and the University of Washington.

The authors would also like to thank the two anonymous referees for their comments on this work.

References

Abazajian, K., and 189 colleagues, 2003. The first data release of the Sloan Digital Sky Survey. Astrophys. J. 126, 2081–2086.
Abazajian, K., and 153 colleagues, 2004. The second data release of the Sloan Digital Sky Survey. Astrophys. J. 128, 502–512.
Abazajian, K., and 154 colleagues, 2005. The third data release of the Sloan Digital Sky Survey. Astrophys. J. 129, 1755–1759.
Adelman-McCarthy, J.K., and 141 colleagues, 2006. The fourth data release of the Sloan Digital Sky Survey. Astrophys. J. Suppl. Ser. 162, 38–48.
Adelman-McCarthy, J.K., and 154 colleagues, 2007. The fifth data release of the Sloan Digital Sky Survey. Astrophys. J. Suppl. Ser. 172, 634–644.
A'Hearn, M.F., Millis, R.L., Schleicher, D.G., Osip, D.J., Birch, P.V., 1995. The ensemble properties of comets: Results from narrowband photometry of 85 comets, 1976–1992. Icarus 118, 223–270.
Dalcanton, J., Kent, S., Okamura, S., Williams, G.V., Tichy, M., Moravec, Z., Koff, R.A., Magnier, G., 1999. Comet C/1999 F2. IAU Circ. 7194, 1.
Emery, J.P., Cruikshank, D.P., van Cleve, J., 2006. Thermal emission spectroscopy (5.238 μm) of three Trojan asteroids with the Spitzer Space Telescope: Detection of fine-grained silicates. Icarus 182, 496–512.
Flaugher, B., 2008. In: Norbert Pirzkal, Henry Ferguson (Eds.), A Decade of Dark Energy: Spring Symposium, Proceedings of the Conferences, May 5–8, 2008, Baltimore, Maryland, USA. Available from: <http://www.stsci.edu/institute/conference/spring2008>.
Fukugita, M., Ichikawa, T., Gunn, J.E., Doi, M., Shimasaku, K., Schneider, D.P., 1996. The Sloan Digital Sky Survey photometric system. Astrophys. J. 111, 1748–1756.
Gunn, J.E., and 40 colleagues, 1998. The Sloan Digital Sky Survey photometric camera. Astrophys. J. 116, 3040–3081.
Gunn, J.E., and 60 colleagues, 2006. The 2.5 m telescope of the Sloan Digital Sky Survey. Astrophys. J. 131, 2332–2359.
Hogg, D.W., Finkbeiner, D.P., Schlegel, D.J., Gunn, J.E., 2001. A photometricity and extinction monitor at the Apache Point Observatory. Astrophys. J. 122, 2129–2138.
Hsieh, H.H., Jewitt, D., 2006. A population of comets in the main asteroid belt. Science 312, 561–563.
Ivezić, Ž., and 32 colleagues, 2001. Solar System objects observed in the Sloan Digital Sky Survey commissioning data. Astrophys. J. 122, 2749–2784.
Ivezić, Ž., and 14 colleagues, 2003. Variability studies with SDSS. Mem. Soc. Astron. Italiana 74, 978–983.
Ivezić, Ž., and 27 colleagues, 2004. SDSS data management and photometric quality assessment. Astron. Nachr. 325, 583–589.
Ivezić, Ž., and 31 colleagues, 2007. Sloan Digital Sky Survey standard star catalog for stripe 82: The dawn of industrial 1% optical photometry. Astrophys. J. 134, 973–998.
Ivezić, Ž., Tyson, J.A., Allsman, R., Andrew, J., Angel, R., and for the LSST Collaboration, 2008. LSST: From science drivers to reference design and anticipated data products. ArXiv:0805.2366.
Jewitt, D.C., Meech, K.J., 1987. Surface brightness profiles of 10 comets. Astrophys. J. 317, 992–1001.
Jurić, M., and 16 colleagues, 2002. Comparison of positions and magnitudes of asteroids observed in the Sloan Digital Sky Survey with those predicted for known asteroids. Astrophys. J. 124, 1776–1787.
Kaiser, N., and 26 colleagues, 2002. Pan-STARRS: A Large Synoptic Survey Telescope Array. In: Tyson, J.A., Wolff, S. (Eds.), Survey and Other Telescope Technologies and Discoveries. Presented at the Society of Photo-Optical Instrumentation Engineers (SPIE) Conference. Proceedings of the SPIE, vol. 4836, pp. 154–164.
Levison, H.F., Duncan, M.J., 1997. From the Kuiper Belt to Jupiter-family comets: The spatial distribution of ecliptic comets. Icarus 127, 13–32.
Lowry, S.C., Fitzsimmons, A., 2001. CCD photometry of distant comets II. A&A 365, 204–213.
Lowry, S.C., Fitzsimmons, A., Cartwright, I.M., Williams, I.P., 1999. CCD photometry of distant comets. A&A 349, 649–659.
Lowry, S.C., Fitzsimmons, A., Collander-Brown, S., 2003. CCD photometry of distant comets. III. Ensemble properties of Jupiter-family comets. A&A 397, 329–343.
Lupton, R.H., Ivezić, Ž., Gunn, J.E., Knapp, G., Strauss, M.A., Yasuda, N., 2002. SDSS imaging pipelines. In: Tyson, J.A., Wolff, S. (Eds.), Survey and Other Telescope Technologies and Discoveries. Presented at the Society of Photo-Optical Instrumentation Engineers (SPIE) Conference. Proceedings of the SPIE, vol. 4836, pp. 350–356.
Parker, A., Ivezić, Ž., Jurić, M., Lupton, R., Sekora, M.D., Kowalski, A., 2008. The size distributions of asteroid families in the SDSS Moving Object Catalog 4. Icarus 198, 138–155.
Pier, J.R., Munn, J.A., Hindsley, R.B., Hennessy, G.S., Kent, S.M., Lupton, R.H., Ivezić, Ž., 2003. Astrometric calibration of the Sloan Digital Sky Survey. Astrophys. J. 125, 1559–1579.

Scranton, R., and 46 colleagues, 2002. Analysis of systematic effects and statistical uncertainties in angular clustering of galaxies from early Sloan Digital Sky Survey data. Astrophys. J. 579, 48–75.

Smith, J.A., and 22 colleagues, 2002. The $u'g'r'i'z'$ standard-star system. Astrophys. J. 123, 2121–2144.

Stokes, G.H., Evans, J.B., Viggh, H.E.M., Shelly, F.C., Pearce, E.C., 2000. Lincoln near-Earth asteroid program (LINEAR). Icarus 148, 21–28.

Stoughton, C., and 192 colleagues, 2002. Sloan Digital Sky Survey: Early data release. Astrophys. J. 123, 485–548.

Strauss, M.A., and 36 colleagues, 2002. Spectroscopic target selection in the Sloan Digital Sky Survey: The main galaxy sample. Astrophys. J. 124, 1810–1824.

Szabó, G.M., Ivezić, Ž., Jurić, M., Lupton, R., 2007. The properties of jovian Trojan asteroids listed in SDSS Moving Object Catalogue 3. MNRAS 377, 1393–1406.

Tucker, D.L., and 34 colleagues, 2006. The Sloan Digital Sky Survey monitor telescope pipeline. Astron. Nachr. 327, 821–843.

York, D.G., and 144 colleagues, 2000. The Sloan Digital Sky Survey: Technical summary. Astrophys. J. 120, 1579–1587.